Topographic/isostatic evaluation of new-generation GOCE gravity field models

C. Hirt,[1] M. Kuhn,[1] W. E. Featherstone,[1] and F. Göttl[2]

Received 19 September 2011; revised 12 March 2012; accepted 19 March 2012; published 11 May 2012.

[1] We use gravity implied by the Earth's rock-equivalent topography (RET) and modeled isostatic compensation masses to evaluate the new global gravity field models (GGMs) from European Space Agency (ESA)'s Gravity Field and Steady-State Ocean Circulation Explorer (GOCE) satellite gravimetry mission. The topography is now reasonably well-known over most of the Earth's landmasses, and also where conventional GGM evaluation is prohibitive due to the lack (or unavailability) of ground-truth gravity data. We construct a spherical harmonic representation of Earth's RET to derive band-limited topography-implied gravity, and test the somewhat simplistic Airy/Heiskanen and Pratt/Hayford hypotheses of isostatic compensation, but which did not improve the agreement between gravity from the uncompensated RET and GOCE. The third-generation GOCE GGMs (based on 12 months of space gravimetry) resolve the Earth's gravity field effectively up to spherical harmonic degree ∼200–220 (∼90–100 km resolution). Such scales could not be resolved from satellites before GOCE. From the three different GOCE processing philosophies currently in use by ESA, the time-wise and direct approaches exhibit the highest sensitivity to short-scale gravity recovery, being better than the space-wise approach. Our topography-implied gravity comparisons bring evidence of improvements from GOCE to gravity field knowledge over the Himalayas, Africa, the Andes, Papua New Guinea and Antarctic regions. In attenuated form, GOCE captures topography-implied gravity signals up to degree ∼250 (∼80 km resolution), suggesting that other signals (originating, e.g., from the crust-mantle boundary and buried loads) are captured as well, which might now improve our knowledge on the Earth's lithosphere structure at previously unresolved spatial scales.

Citation: Hirt, C., M. Kuhn, W. E. Featherstone, and F. Göttl (2012), Topographic/isostatic evaluation of new-generation GOCE gravity field models, *J. Geophys. Res.*, *117*, B05407, doi:10.1029/2011JB008878.

1. Introduction

[2] The Gravity Field and Steady-State Ocean Circulation Explorer (GOCE) is the first core mission of the "Living Planet" Earth observation program by the European Space Agency (ESA) [e.g., *Drinkwater et al.*, 2003]. The GOCE satellite was launched in March 2009 and entered its operational phase in September 2009. GOCE is the first mission to carry a dedicated on-board three-axis gravity gradiometer at a low orbit altitude of ∼260 km [*Bock et al.*, 2011] attempting to resolve Earth's external gravity field with unprecedented detail from space.

[3] GOCE gravity field determination is based on the combination of satellite gravity gradiometry (SGG) with satellite-to-satellite tracking (SST). SGG, used to measure the second derivatives of the gravitational potential, is very sensitive to the medium-wavelength components of the gravity field [e.g., *Rummel et al.*, 2011]. In solid-Earth geophysics, GOCE SGG is expected to resolve regional mass-density anomalies that carry information on the Earth's interior [e.g., *Marotta*, 2003; *Bagherbandi*, 2011; *Reguzzoni and Sampietro*, 2012]. GPS-based SST provides high-accuracy information on the GOCE satellite orbit geometry [*Bock et al.*, 2011] to complement the GOCE SGG in the long wavelengths. GOCE's repeat cycle (the period to achieve full global data coverage) is ∼2 months, and the envisaged data collection period is expected to total ∼40 months, from September 2009 to December 2012 and possibly longer.

[4] GOCE's mission target was to map gravity field features with 1–2 cm accuracy for geoid undulations and ∼1 mgal for gravity, down to scales of ∼100 km, or spherical harmonic degree ∼200. By comparison, geoid undulations from the EGM2008 global geopotential model (GGM) [*Pavlis et al.*, 2008] are estimated to be accurate at the ∼7 cm

[1]Western Australian Centre for Geodesy and Institute for Geoscience Research, Curtin University of Technology, Perth, Western Australia, Australia.
[2]Deutsches Geodätisches Forschungsinstitut, Munich, Germany.

Corresponding author: C. Hirt, Western Australian Centre for Geodesy and Institute for Geoscience Research, Curtin University of Technology, GPO Box U1987, Perth, WA 6845, Australia.
(c.hirt@curtin.edu.au)

0148-0227/12/2011JB008878

Table 1. Global Gravity Field Models Tested

Model Name	Degree	GOCE Data	Other Data[i]	Reference
GOCE-DIR3[a]	240	∼12 months	LAGEOS and GRACE to degree 160 from GRGS RL02 [*Bruinsma et al*., 2010b]	*Bruinsma et al*. [2010a]
GOCE-DIR2[b]	240	8 months	ITG-Grace2010s to degree 150	*Bruinsma et al*. [2010a]
GOCE-DIR1[c]	240	2 months	EIGEN51C (GRACE, CHAMP, G,A) at all scales	*Bruinsma et al*. [2010a]
GOCE-SPW2[d]	240	8 months	N/A	*Migliaccio et al*. [2010]
GOCE-SPW1[e]	210	2 months	EGM2008 (GRACE, G,A) at low degrees	*Migliaccio et al*. [2010]
GOCE-TIM3[f]	250	∼12 months	N/A	*Pail et al*. [2011]
GOCE-TIM2[g]	250	8 months	N/A	*Pail et al*. [2011]
GOCE-TIM1[h]	224	2 months	N/A	*Pail et al*. [2010]
ITG-Grace2010s	180	-	7 years GRACE	ITG-Grace2010 (http://www.igg.uni-bonn.de/apmg/index.php?id=itg-grace2010)

[a]ESA name: GO_CONS_EGM_GCF_2__20091101T000000_20110419T235959_0001; ICGEM name GOC_CONS_GCF_2_DIR_R3.
[b]ESA name: GO_CONS_EGM_DIR_2I_20091101T000000_20100630T235959_0001; ICGEM name GOC_CONS_GCF_2_DIR_R2.
[c]ESA name: EGM_GOC_2__20091101T000000_20100110T235959_0002; ICGEM name GOC_CONS_GCF_2_DIR_R1.
[d]ESA name: GO_CONS_EGM_SPW_2I_20091031T000000_20100705T235959_0001; ICGEM name: GOC_CONS_GCF_2_SPW_R2.
[e]ESA name: EGM_GOC_2__20091030T005757_20100111T073815_0002; ICGEM name: GOC_CONS_GCF_2_SPW_R1.
[f]ESA name: GO_CONS_EGM_GCF_2__20091101T000000_20110430T235959_0001; ICGEM name: GOC_CONS_GCF_2_TIM_R3.
[g]ESA name: GO_CONS_EGM_TIM_2I_20091101T000000_20100705T235500_0001; ICGEM name: GOC_CONS_GCF_2_TIM_R2.
[h]ESA name: EGM_GOC_2__20091101T000000_20100111T000000_0002; ICGEM name: GOC_CONS_GCF_2_TIM_R1.
[i]Abbreviations: G = terrestrial gravity, A = gravity from altimetry.

level (global RMS). Over gravimetrically well-surveyed areas, the EGM2008 geoid accuracy can be at the level of some cm [e.g., *Hirt et al.*, 2010a], while the accuracy degrades to the dm-level over large parts of Asia, Africa, South America and Antarctica [*Pavlis et al.*, 2008]. In these EGM2008 "problem areas," *Pavlis et al.* [2008] did not have high-resolution terrestrial gravity data (12% of land) or only had access to proprietary data (43% of land). It is these regions devoid of dense sets of terrestrial gravity observations where GOCE is expected to add most significantly to terrestrial gravity field knowledge.

[5] ESA has made available GOCE GGMs based on ∼2 months (herein first-generation), ∼8 months (second-generation) and ∼12 months (third-generation) of observation data, based on three different strategies for gravity field recovery [e.g., *Pail et al.*, 2011] (see section 2). The performance of the first-generation GGMs has been evaluated by different strategies. *Gruber et al.* [2011] investigated GOCE-implied orbit residuals of various geodetic satellites and compared GOCE GGMs against ground-truth geoid undulations. *Hirt et al.* [2011] utilized regional land gravity and vertical deflections as ground-truth to assess GOCE gravity field information. Differences between GOCE GGMs and EGM2008 (from the pre-GOCE-era) were analyzed by *Hirt et al.* [2011] and *Pail et al.* [2011], and inferences were made but no direct evidence obtained for GOCE-conferred improvements over the EGM2008 'problem areas'.

[6] The aim of this study is to use gravity implied by the Earth's topography and models of its isostatic compensation masses to assess the new-generation GOCE model performance over the Himalayas, Africa, Andes, Papua New Guinea and Antarctica. We exploit the relatively good knowledge of topography over most of the Earth's surface (through digital elevation models) along with GOCE's sensitivity to the gravitational attraction of topographic masses [*Wild and Heck*, 2005; *Makhloof and Ilk*, 2008; *Janák et al.*, 2012] to bring—for the first time—direct evidence for GOCE gravity field improvements in regions where terrestrial gravity data are restricted.

[7] Based on topographic heights over land areas, ocean depths, ice shield thickness data, we construct rock-equivalent topography (RET) [*Rummel et al.*, 1988] and derive RET-implied gravity to approximate the gravitational attraction of Earth's topography and some of Earth's major mass-density anomalies. Some focus is placed on ways to account for isostatic compensation of the topography [e.g., *Watts*, 2001]. The gravitational effect from the isostatic compensation masses is approximated and tested here based on the Crust 2.0 lithosphere model [*Bassin et al.*, 2000], the classical Airy/Heiskanen and Pratt/Hayford hypotheses and a combination of them (section 3). The relationship between GOCE-measured and topography/isostasy-implied gravity is not only analyzed using correlation coefficients, but also based on a new criterion termed reduction rates. These quantify the extent of topography-implied gravity signals captured by the GOCE GGMs at different spatial scales (i.e., as a function of harmonic degree). Reduction rates are introduced and used because they are more sensitive than correlation coefficients to identify topography-generated signals in the GGMs (section 4).

[8] Gravity implied by RET not only allows for identification of GOCE-conferred gravity field improvements over EGM2008 "problem areas," but also global and regional evaluation of the GOCE gravity recovery strategies. Using RET as a single, globally homogeneous reference data set, our analyses provide independent feedback on the ability of the ESA GOCE gravity processing strategies to recover short-scale gravity signals. While *Pail et al.* [2011, p. 840] state that "due to the fact that the [three] models are based on different processing philosophies … they cannot and should

not be compared directly," we believe that users are interested to know how the different GOCE models perform both in an absolute and relative sense. Comparisons between uncompensated and compensated RET demonstrate that the classical hypotheses of isostatic compensation are of limited use to model isostasy globally at the spatial scales resolved by GOCE. Comparisons with uncompensated RET-implied gravity show the performance differences of the three GOCE gravity recovery strategies, and demonstrate the sensitivity of GOCE gradiometry for short-scale gravity recovery at spatial scales down to ~80 km, which also has future applications in solid Earth geophysics, e.g., the improvement of lithosphere models at short scales (sections 4 and 5).

2. Data Sets

2.1. GOCE Gravity Field Models

[9] The spherical harmonic coefficients of eight GOCE-based GGMs from the GOCE High-Level Processing Facility (HPF) have been released publically via ESA (http://www.esa.int) and the International Centre for Global Earth Models (ICGEM, http://icgem.gfz-potsdam.de/ICGEM/). Table 1 gives an overview of their formal resolution (i.e., the maximum spherical harmonic degree published), the data used to derive the model coefficients, and the corresponding citations. As a benchmark of the pre-GOCE-era, one GRACE (Gravity and Climate Change Experiment [*Tapley et al.*, 2004])-based model (ITG-GRACE2010s, using seven years of GRACE observations; http://www.igg.uni-bonn.de/apmg/index.php?id=itg-grace2010) is also included.

[10] The eight GOCE GGMs are based on three different processing philosophies [*Pail et al.*, 2011]: the direct approach (DIR), space-wise approach (SPW) and time-wise approach (TIM). Each approach has been applied to ~2 months (first-generation), ~8 months (second-generation) and ~12 months (third-generation) of GOCE gradiometry and GPS-derived orbits. Below are the basic concepts and most important differences among the approaches, inferred from *Pail et al.* [2011] and the header information in the coefficient files from ICGEM.

[11] 1. The DIR and TIM approaches use the least squares solution of the inverse problem, where GOCE observations (gradiometry and GPS orbits) are related to the unknown parameters (spherical harmonic coefficients of Earth's gravity field) via large systems of normal equations. Their direct inversion generally requires the use of supercomputers.

[12] 2. The DIR-approach makes use of an a priori GGM (cf. Table 1) and adds GOCE observations to improve it. An important difference between first- and second/third-generation DIR models, GOCE-DIR1 incorporates a priori information from the combined EIGEN-51C model [*Bruinsma et al.*, 2010a] at all spatial scales. As such, GOCE-DIR1 relies on other satellite data at long scales and terrestrial gravity at short scales. Opposed to this, GOCE-DIR2 uses the GRACE-only derived model ITG-GRACE2010s (cf. Table 1) as an a priori GGM to degree 150, so is a pure GOCE-only GGM beyond this degree. GOCE-DIR3 uses LAGEOS Satellite Laser Ranging and the GRGS GRACE model [*Bruinsma et al.*, 2010b] gravity field as an a priori to degree 160.

[13] 3. No a priori gravity field information is used in the GGMs derived from the TIM approach, but Kaula regularization (an empirical law on the decay of the Earth's gravity spectrum with altitude [cf. *Kaula*, 1966]) is applied to constrain the TIM1, TIM2 and TIM3 GGM coefficients at short scales. The TIM processing philosophy delivers pure GOCE-only models that are independent of a priori gravity field data.

[14] 4. In the SPW approach, GOCE observations are gridded at satellite altitude by means of least squares collocation. The spherical harmonic coefficients are obtained through a spherical harmonic analysis of the gridded observations. EGM2008 is incorporated into GOCE-SPW1 as an a priori model only at very long wavelengths, so it can be considered as a pure GOCE-only model at medium and shorter scales. According to the ICGEM file information, GOCE-SPW2 does not use a priori gravity field information. GOCE-SPW3 is not yet publicly available.

[15] In summary, GOCE-TIM1,2&3 and GOCE-SPW2 are pure GOCE-only models at all spatial scales, and GOCE-SPW1 is GOCE-only apart from the very long wavelengths. GOCE-DIR2&3 are GOCE-only models at short scales and GOCE-DIR1 is a mixed product that is underpinned by various prior gravity field sources.

[16] We acknowledge that "combined satellite-only" GGMs (e.g., GOCO01S [*Pail et al.*, 2010], GOCO02S [*Goiginger et al.*, 2011], and EIGEN-6 [*Förste et al.*, 2011]) have been developed based on GOCE and GRACE. Such GGMs are superior to GOCE-only models due to incorporating highly accurate GRACE models at long wavelengths (and/or other satellite data) [cf. *Pail et al.*, 2010]. Given that the GOCE component of these combined satellite-only GGMs is similar or identical to the ESA GOCE products, we limit our study to the GGMs in Table 1.

2.2. Topography

[17] We use the spherical harmonic expansion of the DTM2006.0 digital elevation data [*Pavlis et al.*, 2007], a co-product of EGM2008 [*Pavlis et al.*, 2008]. It contains (i) the Shuttle Radar Topography Mission (SRTM) [*Farr et al.*, 2007] data over land within latitudes of 56° South and 60° North, (ii) ICESat-2 laser altimetry [*Abdalati et al.*, 2010] over Greenland and Antarctica, (iii) bathymetry derived from altimetry and ship depth soundings [*Smith and Sandwell*, 1997], and (iv) DTM2002 elevation data [*Saleh and Pavlis*, 2003] elsewhere. Spherical harmonic coefficients of the topography, derived to degree 2700 from $2' \times 2'$ DTM2006.0 mean values, are publicly available to degree 2160 via http://earth-info.nga.mil/GandG/wgs84/gravitymod/egm2008/.

[18] In order to better RET-model the ice sheets over Greenland and Antarctica, we use the bedrock information contained in the global $1' \times 1'$ ETOPO1 relief model [*Amante and Eakins*, 2009]. Over Greenland, bedrock elevations are obtained indirectly through ice surface and ice thickness information provided by the National Snow and Ice Data Centre (NSIDC) [*Bamber et al.*, 2001]. The ice surface is the result of the combination of radar altimetry and airborne data, where the ice thickness is obtained from airborne ice-penetrating radar. Over Antarctica, BEDMAP describes the bedrock elevation under the grounded ice

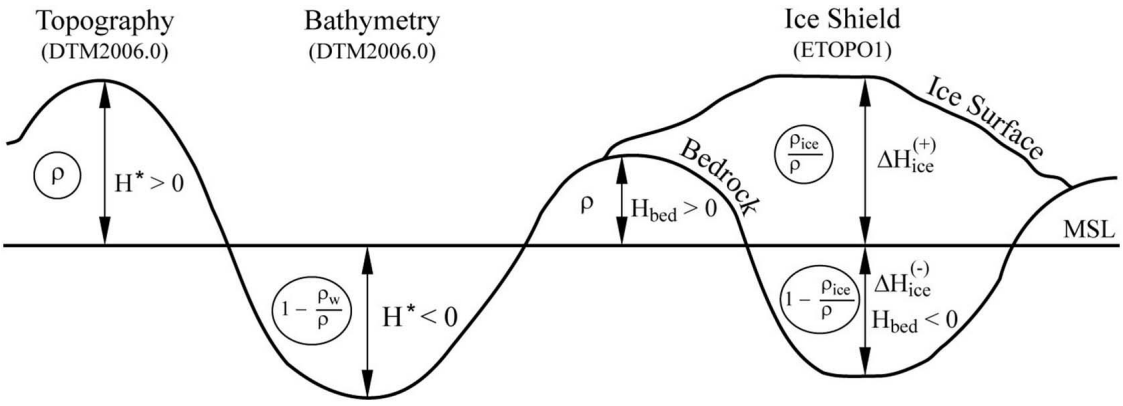

Figure 1. Terrain types used to construct the rock-equivalent topography RET2011 heights.

sheets [*Lythe et al.*, 2000]. This is based primarily on the gridding of radar and seismic soundings.

3. Methodology

3.1. Introductory Remarks

[19] The basic idea of this study is to compare gravity signals, as measured by GOCE and implied by Earth's topography and models of its isostatic compensating masses, at various spatial scales. For this purpose, we construct a spherical harmonic representation of Earth's topography, cryosphere and hydrosphere based on a uniform mass-density (section 3.2), derive its gravitational potential (section 3.3) and gravity disturbances (section 3.4) that are compared with GOCE over a range of spectral bands (section 4), allowing us analyses of GOCE's sensitivity for topography-generated gravity signals, specifically at short spatial scales that have never been measured from space before.

[20] GOCE is not only sensitive to the gravitational attraction of the Earth's visible topography, but also to its isostatic compensation masses [e.g., *Wild and Heck*, 2005; *Makhloof and Ilk*, 2008]. This raises the question of how to account for isostatic compensation in the comparisons between GOCE and Earth's topography. An initial strategy is to consider the topography as isostatically uncompensated or supported by the rigidity of the lithosphere, which, according to *Wieczorek* [2007], should be a "good approximation" above harmonic degree ∼200. To model isostatic compensation of the topographic masses, commonly used strategies are available that are based on the following:

[21] 1. Simplistic compensation models, such as those of Airy-Heiskanen (A/H) or Pratt-Hayford (P/H) [e.g., *Heiskanen and Moritz*, 1967; *Torge*, 2001; *Göttl and Rummel*, 2009]. The A/H and P/H models (section 3.3) assume local compensation of the topography loads and an intrinsically weak crust [e.g., *Watts*, 2001], so are sometimes crude simplifications of the actual lithospheric properties. It is important to note that both the A/H and P/H compensation models offer (formally) a spatial resolution comparable to that of the topography model, so possess short-scale spectral energy, which is a prerequisite for comparisons with GOCE.

[22] 2. More regional compensation models of Vening-Meinesz also take into account the flexural rigidity of the lithosphere [e.g., *Watts*, 2011]. Regional compensation models imply that loads larger than a certain transition wavelength are compensated, while smaller topographic features are supported mechanically by the lithosphere. The transition wavelength depends upon, among other parameters, the elastic thickness T_e.

[23] 3. Crustal thicknesses estimates can be obtained, e.g., from seismic refraction data such as the Crust 2.0 lithosphere model [*Bassin et al.*, 2000], or effective elastic thickness estimates from admittance and coherence studies [e.g., *Watts*, 2001, p. 416f]. However, neither the Crust 2.0 resolution ($2^\circ \times 2^\circ$ corresponding to spherical harmonic degree of 90), nor the resolution or accuracy of global elastic thickness maps [see *Watts*, 2001, p. 418] are of sufficient resolution to provide feedback on GOCE observations at ∼100 km spatial scales (equivalent to harmonic degree of 200).

[24] To our knowledge, there is currently no global crustal thickness model available of sufficient resolution that would allow us to account for and model isostatic compensation effects at or near the GOCE spatial resolution of ∼100 km, without having to rely on simplified hypotheses such as those behind the A/H or P/H models. Vening-Meinesz-type models rely on the core assumption that local topographic loads are supported mechanically by the lithosphere, so are very similar to the uncompensated topography (option 1 below) at short spatial scales, and are not included here. The limited resolution of crustal thickness models (option 5 below) is exemplified in section 4.2. In the absence of "observation-based" crustal thickness models of sufficiently high spatial resolution, we are restricted to test the following five modeling variants of Earth's topography and its isostatic compensation: (1) uncompensated (rock-equivalent) topography, ice and oceans, (2) A/H isostatic compensation plus the effect of option 1, (3) P/H isostatic compensation plus the effect of option 1, (4) A combination of A/H and P/H, that uses A/H over the continents and P/H over the oceans, plus the effect of option 1, and (5) the Crust 2.0 lithosphere model.

[25] Also because of the lack of a high-resolution 3D density model of the crust and lithosphere, we are unable to account for the isostatic compensation of mass anomalies.

3.2. Rock-Equivalent Topography

[26] RET is a representation of Earth's topography that "compresses" ocean water and ice into layers equivalent to the mass-density of topographic rock (using the frequently

presumed mean value of 2670 kg m^{-3}), while keeping the water and ice masses constant. RET allows computation of implied gravity effects based on a single constant uniform mass-density over land, ocean areas and ice shields.

[27] For our topography-based GOCE GGM evaluation, RET is required in a spherical harmonic representation. The published version of DTM2006.0 [*Pavlis et al.*, 2007] (http://earth-info.nga.mil/GandG/wgs84/gravitymod/egm2008/first_release.html) cannot be used directly because it describes the surface of the solid Earth above or below local mean sea level. Over Greenland and Antarctica, DTM2006.0 heights are reckoned to the top of the ice shields so the incorrect RET would be assigned to ice masses; likewise for the oceans. As such, the scheme depicted in Figure 1 is used to appropriately assign mass densities to ice and ocean water. We have constructed a RET in the spatial domain that accounts for the effect of the ocean water masses and ice shields over Greenland and Antarctica, and derived its spherical harmonic coefficients. The construction, which we name RET2011, was based on following three-step procedure.

[28] First, a 5′ × 5′ global grid of DTM2006.0 heights H^* to maximum degree $n_{\max}^{DTM2006} = 2160$ was computed using the spherical harmonic expansion (http://earth-info.nga.mil/GandG/wgs84/gravitymod/egm2008):

$$H^* = \sum_{n=0}^{n_{\max}^{DTM2006}} \sum_{m=0}^{n} \left(\overline{HC}^*_{nm} \cos m\lambda + \overline{HS}^*_{nm} \sin m\lambda\right) \bar{P}_{nm}(\cos\theta) \quad (1)$$

where $\overline{HC}^*_{nm}$ and $\overline{HS}^*_{nm}$ are the 4π-fully normalized spherical harmonic coefficients of the DTM2006.0 database, $\bar{P}_{nm}(\cos\theta)$ are the 4π-fully normalized associated Legendre functions of degree n and order m, and λ longitude and θ geocentric co-latitude of the computation point.

[29] Second, the grid of DTM2006.0 H^* was converted to RET elevations H by transforming the ocean depths using [*Rummel et al.*, 1988; *Wieczorek*, 2007]

$$H = \begin{cases} H^*(1 - \rho_W/\rho) & , H^* < 0 \\ H^* & , H^* \geq 0 \end{cases} \quad (2)$$

where ρ_W is the mean mass-density of ocean water (1030 kg m^{-3}) and ρ the mean mass-density of topographic rock (2670 kg m^{-3}). This reduction of ocean depths by factor $(1 - \rho_W/\rho) = 0.614$ compresses the ocean water into RET. Over Greenland and Antarctica DTM2006.0 heights represent the interface between ice and air, thus additional information on the bedrock underneath the ice shields is required to properly model the RET. Over these areas, DTM2006 was replaced by ETOPO1 (area-weight-averaged to a 5′ × 5′ grid) which has been used to obtain RET heights through

$$H = H_{bed} + \Delta H_{ice}^{(-)} \left(1 - \frac{\rho_{ice}}{\rho}\right) + \Delta H_{ice}^{(+)} \frac{\rho_{ice}}{\rho} \quad (3)$$

where H_{bed} is the bedrock height, ρ_{ice} is the mean mass-density of ice (927 kg m^{-3}) and $\Delta H_{ice}^{(+)}$ and $\Delta H_{ice}^{(-)}$ are the thicknesses of ice masses above and below mean sea level (MSL), cf. Figure 1. Equation (3) is valid for bedrock above MSL (e.g., $H_{bed} \geq 0$) and below MSL (e.g., $H_{bed} < 0$). The thickness $\Delta H_{ice}^{(+)}$ of ice masses above MSL are reduced by the factor $\rho_{ice}/\rho = 0.347$ and the thickness $\Delta H_{ice}^{(-)}$ of ice masses below MSL are reduced by the factor $(1 - \rho_{ice}/\rho) = 0.653$.

[30] Third, the 5′ × 5′ grid of RET H was analyzed harmonically to yield spherical harmonic coefficients $\overline{HC}_{nm}$, $\overline{HS}_{nm}$ of RET2011. Though the GGM evaluation requires the $\overline{HC}_{nm}$, $\overline{HS}_{nm}$ coefficients only to degree 250, we derived $\overline{HC}_{nm}$, $\overline{HS}_{nm}$ to degree 360 which can be used for RET-based evaluation of future GGMs. Our spherical harmonic analysis is based on least squares estimation of the harmonic coefficients [e.g., *Colombo*, 1981; *Torge*, 2001, p. 272]. Following this approach, a regular global grid of RET heights (symmetric to the equator) is used to develop grid elements along the same parallel into Fourier series in sin $m\lambda$ and cos $m\lambda$. Based on the Fourier series coefficients the 4π fully normalized spherical harmonic coefficients $\overline{HC}_{nm}$, $\overline{HS}_{nm}$ are obtained through least squares estimation. RET2011 heights expanded to degree 250 (the maximum resolution of the second generation GOCE models) are shown in Figure 2.

3.3. Potential Coefficients

3.3.1. Uncompensated RET

[31] The $\overline{HC}_{nm}$, $\overline{HS}_{nm}$ coefficients of RET2011 were converted into gravitational potential spherical coefficients $\overline{C}_{nm}^{\mathrm{RET}}$ $\overline{S}_{nm}^{\mathrm{RET}}$ using [*Rummel et al.*, 1988; *Kuhn and Featherstone*, 2003]

$$\begin{Bmatrix} \overline{C}_{nm}^{RET} \\ \overline{S}_{nm}^{RET} \end{Bmatrix} = \frac{3}{2n+1} \cdot \frac{\rho}{\overline{\rho}} \left[\begin{Bmatrix} \overline{HC1}_{nm} \\ \overline{HS1}_{nm} \end{Bmatrix} + \frac{n+2}{2} \begin{Bmatrix} \overline{HC2}_{nm} \\ \overline{HS2}_{nm} \end{Bmatrix} + \frac{(n+2)(n+1)}{6} \begin{Bmatrix} \overline{HC3}_{nm} \\ \overline{HS3}_{nm} \end{Bmatrix} \right] \quad (4)$$

with $\overline{\rho}$ mean mass-density of Earth (5515 kg m^{-3}) and ρ the mean mass-density of topographic rock (2670 kg m^{-3}). $\overline{HC1}_{nm}, \overline{HS1}_{nm}$ are the spherical harmonic coefficients of the dimensionless surface function $H1 := H/R$ and obtained from

$$\begin{aligned} \overline{HC1}_{nm} &= \overline{HC}_{nm}/R \\ \overline{HS1}_{nm} &= \overline{HS}_{nm}/R \end{aligned} \quad (5)$$

where R is the equatorial Earth radius of 6378137 m [*Torge*, 2001]. $\overline{HC2}_{nm}, \overline{HS2}_{nm}$ denote the spherical harmonic coefficients of surface function $H2$:

$$H2 := \left(\frac{H}{R}\right)^2 = \sum_{n=0}^{360} \sum_{m=0}^{n} \left(\overline{HC2}_{nm} \cos m\lambda + \overline{HS2}_{nm} \sin m\lambda\right) \cdot \bar{P}_{nm}(\cos\theta) \quad (6)$$

and $\overline{HC3}_{nm}, \overline{HS3}_{nm}$ are the coefficients of surface function $H3$:

$$H3 := \left(\frac{H}{R}\right)^3 = \sum_{n=0}^{360} \sum_{m=0}^{n} \left(\overline{HC3}_{nm} \cos m\lambda + \overline{HS3}_{nm} \sin m\lambda\right) \cdot \bar{P}_{nm}(\cos\theta) \quad (7)$$

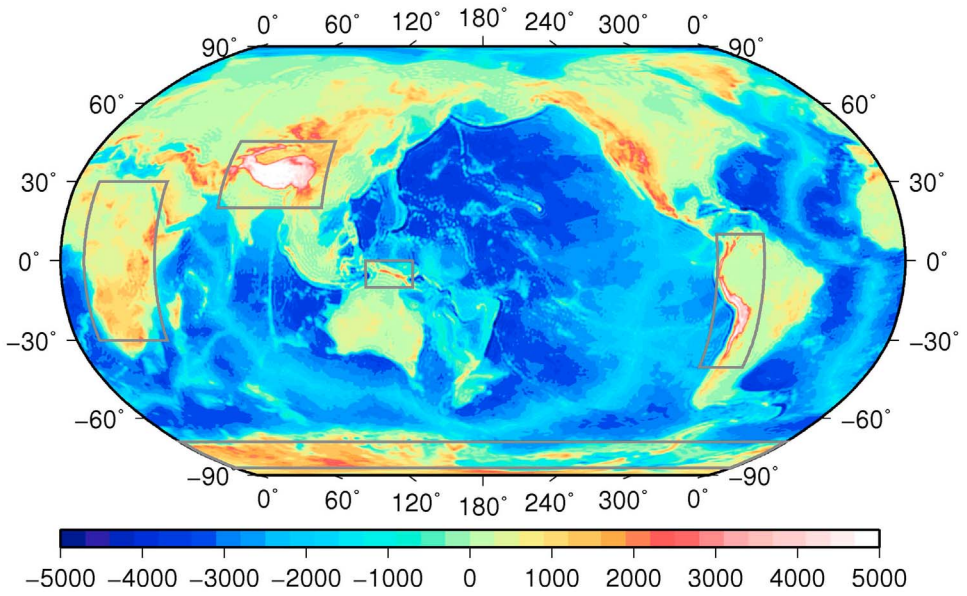

Figure 2. Earth's rock-equivalent topography RET2011 to spherical harmonic degree 250. Robinson projection, units in meters. Grey boxes show evaluation regions used in section 4.

For evaluation of equation (4), $\overline{HC1}_{nm}, \overline{HS1}_{nm}$ are readily available from equation (5), while two additional spherical harmonic analyses are needed to derive the coefficients $\overline{HC2}_{nm}, \overline{HS2}_{nm}$ and $\overline{HC3}_{nm}, \overline{HS3}_{nm}$ of the surface functions $H2$ and $H3$, respectively. The surface functions $H2$ and $H3$ are computed as a function of H (equations (6) and (7)) after the H were synthesized on a high-resolution grid using

$$H = \sum_{n=0}^{360} \sum_{m=0}^{n} \left(\overline{HC}_{nm} \cos m\lambda + \overline{HS}_{nm} \sin m\lambda\right) \bar{P}_{nm}(\cos\theta) \qquad (8)$$

Equation (4) is a series expansion to third-order of H, which is obtained by replacing the inverse distance in Newton's integral through a series of Legendre polynomials [e.g., *Heiskanen and Moritz*, 1967, p. 32]. A first-order expansion delivers well above 90% of the overall topography-implied gravity signal [cf. *Novák and Grafarend*, 2006, Figure 3]. With any additional term, topography-implied signal captured by the $\overline{C}_{nm}^{RET}\,\overline{S}_{nm}^{RET}$ potential coefficients comes closer to 100% and the contribution of every additional term is smaller than the previous [*Wieczorek*, 2007]. According to *Wieczorek* [2007, Figure 9], the maximum (truncation) error of a third-order expansion is a few mGal, and the average root mean square (RMS) error is well below the mGal-level. Given that the global RMS gravity signal strength is ∼35 mGal (http://earth-info.nga.mil/GandG/wgs84/gravitymod/egm2008), the third-order expansion appears sufficient.

3.3.2. Airy-Heiskanen Compensation

[32] In the A/H model, a lighter lithosphere is assumed to float on a denser mantle, and isostatic compensation is assumed to take place locally in vertical columns of equal mass-density [e.g., *Heiskanen and Moritz*, 1967; *Watts*, 2001, *Torge*, 2001]. As a consequence, the depth of the sub-surface compensation mass is directly related to the height of the topography ("local compensation"), and the spatial resolution of the A/H compensation model is (formally) identical to the resolution of the topographic model used. The potential coefficients of the A/H-compensated RET are computed from a series expansion to third-order [*Rummel et al.*, 1988, equation 24]:

$$\begin{aligned}\begin{Bmatrix} \overline{C}_{nm}^{A/H} \\ \overline{S}_{nm}^{A/H} \end{Bmatrix} = \frac{3}{2n+1} \cdot \frac{\rho}{\overline{\rho}} \Bigg[\left[1 - \left(\frac{R-T}{R}\right)^{n}\right] \begin{Bmatrix} \overline{HC1}_{nm} \\ \overline{HS1}_{nm} \end{Bmatrix} \\ + \frac{n+2}{2} \left[1 + \frac{\rho}{\rho_m - \rho} \left(\frac{R-T}{R}\right)^{n-3}\right] \begin{Bmatrix} \overline{HC2}_{nm} \\ \overline{HS2}_{nm} \end{Bmatrix} \\ + \frac{(n+2)(n+1)}{6} \left[1 - \left(\frac{\rho}{\rho_m - \rho}\right)^{2} \left(\frac{R-T}{R}\right)^{n-6}\right] \\ \cdot \begin{Bmatrix} \overline{HC3}_{nm} \\ \overline{HS3}_{nm} \end{Bmatrix} \Bigg] \end{aligned} \qquad (9)$$

where T denotes the mean depth of compensation and ρ_m the mass-density of the mantle. Here we use $T = 30$ km and $\rho_m = 3270$ kg m^{-3} [*Torge*, 2001, p. 341]. The potential coefficients $\overline{C}_{nm}^{A/H}, \overline{S}_{nm}^{A/H}$ contain the effect both of the topography and of the A/H-compensation masses. The practical computation of the $\overline{C}_{nm}^{A/H}, \overline{S}_{nm}^{A/H}$ is straightforward as the required sets of potential coefficients of the uncompensated RET ($\overline{HC1}_{nm}, \overline{HS1}_{nm}$, $\overline{HC2}_{nm}, \overline{HS2}_{nm}$ and $\overline{HC3}_{nm}, \overline{HS3}_{nm}$) are readily available from section 3.3.1. We acknowledge that the value of $T = 30$ km is not valid for oceans, so a combination is trialed later (section 3.3.4).

3.3.3. Pratt/Hayford Compensation

[33] The P/H isostatic compensation uses a constant depth of compensation along with laterally varying mass-densities of vertical columns [e.g., *Watts*, 2001; *Torge*, 2001]. A

compact formulation of the potential coefficients $\overline{C}_{nm}^{P/H}$, $\overline{S}_{nm}^{P/H}$ of the P/H-compensated topography is given by *Göttl and Rummel* [2009] as

$$\begin{Bmatrix} \overline{C}_{nm}^{P/H} \\ \overline{S}_{nm}^{P/H} \end{Bmatrix} = \frac{3}{2n+1} \cdot \frac{\rho}{\overline{\rho}} \left[\begin{Bmatrix} \overline{hC1}_{nm} \\ \overline{hS1}_{nm} \end{Bmatrix} + \frac{n+2}{2} \begin{Bmatrix} \overline{hC2}_{nm} \\ \overline{hS2}_{nm} \end{Bmatrix} \cdot \frac{(n+2)(n+1)}{6} \begin{Bmatrix} \overline{hC3}_{nm} \\ \overline{hS3}_{nm} \end{Bmatrix} \right] + \frac{3}{(2n+1)(n+3)} \frac{\rho}{\overline{\rho}} \cdot \left[1 - \left(\frac{R-D}{R} \right)^{n+3} \right] \begin{Bmatrix} \overline{\rho C}_{nm} \\ \overline{\rho S}_{nm} \end{Bmatrix} \quad (10)$$

where D is the depth of compensation [here 100 km], $\overline{\rho}$ mean mass-density of Earth (5515 kg m^{-3}), ρ the mean mass-density of topographic rock (2670 kg m^{-3}). The $\overline{hC1}_{nm}, \overline{hS1}_{nm}$, $\overline{hC2}_{nm}, \overline{hS2}_{nm}$, and $\overline{hC3}_{nm}, \overline{hS3}_{nm}$ are the spherical harmonic coefficients of the dimensionless height function h/R times the dimensionless density function ρ_i/ρ and $\overline{\rho C}_{nm}$, $\overline{\rho S}_{nm}$ are the spherical harmonic coefficients of the dimensionless density function ρ_i/ρ [*Mladek*, 2006, p. 74]:

$$h1 := \left(\frac{h}{R} \frac{\rho_i}{\rho} \right) = \sum_{n=0}^{360} \sum_{m=0}^{n} \left(\overline{hC1}_{nm} \cos m\lambda + \overline{hS1}_{nm} \sin m\lambda \right) \cdot \bar{P}_{nm}(\cos\theta) \quad (11)$$

$$h2 := \left(\frac{h}{R} \frac{\rho_i}{\rho} \right)^2 = \sum_{n=0}^{360} \sum_{m=0}^{n} \left(\overline{hC2}_{nm} \cos m\lambda + \overline{hS2}_{nm} \sin m\lambda \right) \cdot \bar{P}_{nm}(\cos\theta) \quad (12)$$

$$h3 := \left(\frac{h}{R} \frac{\rho_i}{\rho} \right)^3 = \sum_{n=0}^{360} \sum_{m=0}^{n} \left(\overline{hC3}_{nm} \cos m\lambda + \overline{hS3}_{nm} \sin m\lambda \right) \cdot \bar{P}_{nm}(\cos\theta) \quad (13)$$

$$\rho 1 := \frac{\rho_i}{\rho} = \sum_{n=0}^{360} \sum_{m=0}^{n} \left(\overline{\rho C}_{nm} \cos m\lambda + \overline{\rho S}_{nm} \sin m\lambda \right) \bar{P}_{nm}(\cos\theta) \quad (14)$$

Variable h denotes the equivalent rock heights of the P/H model and ρ_i are the [individual] mass-densities of the vertical columns. According to *Göttl and Rummel* [2009] the P/H equivalent rock heights h are determined via

$$h = \begin{cases} H & , H^* \geq 0 \\ \left(\dfrac{\rho (R+H^*)^3 \left[-R^3 + (R-D)^3 \right] - \rho_W (R-D)^3 \left[-R^3 + (R+H^*)^3 \right]}{\rho_W \left[R^3 - (R+H^*)^3 \right] - \rho \left[R^3 - (R-D)^3 \right]} \right)^{1/3} - R & , H^* < 0 \end{cases} \quad (15)$$

where H are the RET2011 heights [from equations (2) and (3)], H^* are the DTM2006 bathymetric depths/topographic heights, and ρ_W is the mean mass-density of ocean water (1030 kg m^{-3}). Equation (15) is the formulation of the P/H equilibrium condition over the oceans [*Göttl and Rummel*, 2009, p. 1253]. Over land areas, RET2011 heights H (topography or ice) and h are identical, while H and h are different over the oceans. Note that *Göttl and Rummel* [2009] used a different sign convention for bathymetric depths. The individual mass-densities ρ_i are obtained from

$$\rho_i = \rho \left(\frac{R^3 - (R-D)^3}{(R+h)^3 - (R-D)^3} \right) \quad (16)$$

For the practical computation of the P/H-compensated RET, we back-converted the RET2011 heights to bathymetric depths H^* over the oceans, and applied equation (15) to obtain rock-equivalent heights h, consistent with the P/H equilibrium condition. We then computed the individual mass-densities ρ_i (equation (16)) of the 5′ × 5′ grid, and analyzed harmonically the dimensionless linear, squared and cubic height functions $h1$, $h2$, $h3$ (equations (11)–(13)). A further harmonic analysis of the 5′ × 5′ grid of $\rho 1$ (equation (14)) yielded the $\overline{\rho C}_{nm}$, $\overline{\rho S}_{nm}$ coefficients required to finally obtain the $\overline{C}_{nm}^{P/H}$ and $\overline{S}_{nm}^{P/H}$ potential coefficients of the P/H compensated RET (equation (10)). The potential coefficients $\overline{C}_{nm}^{P/H}$, $\overline{S}_{nm}^{P/H}$ contain the effect both of the topography and of the P/H-compensation masses.

3.3.4. Combined A/H and P/H Compensation Model

[34] *Göttl and Rummel* [2009] analyzed A/H and P/H compensated gravity anomalies over land and ocean areas and found that the A/H is better suited than P/H to model the isostatic compensation of large mountain chains, while their analysis suggests that P/H is a better approximate description of isostasy over deep ocean trenches. We therefore combine the classical A/H (section 3.3.2) and P/H (section 3.3.3) hypotheses, by using A/H over land areas and P/H over the oceans. A/H and P/H are combined in the spatial domain by using gravity implied by the P/H-compensated topography at points where $H^* < 0$ and the A/H-compensated topography elsewhere, see also *Wild and Heck* [2005] and *Makhloof* [2007], who used the same combination strategy. "By this mixture, one of the drawbacks of the original Airy-Heiskanen model – the fact that the antiroots may rise above the ocean bottom in deep sea trough areas – can be avoided." [*Wild and Heck*, 2005, p. 233].

3.4. Gravity Computations

[35] Gravity disturbances δg^{GGM} from each GGM were computed at points specified by radius r, longitude λ and geocentric co-latitude θ from the spherical harmonic coefficients $\overline{C}_{nm}^{GGM}$ $\overline{S}_{nm}^{GGM}$ of the various GOCE GGMs via [*Heiskanen and Moritz*, 1967; *Torge*, 2001]

$$\delta g^{GGM} = \frac{GM^{GGM}}{r^2}\sum_{n=n_1}^{n_2}\left(\frac{a^{GGM}}{r}\right)^n (n+1)\sum_{m=0}^{n}\left(\overline{C}_{nm}^{GGM}\cos m\lambda + \overline{S}_{nm}^{GGM}\sin m\lambda\right)\bar{P}_{nm}(\cos\theta) \quad (17)$$

where a_{GGM} (model scale factor) and GM_{GGM} (gravitational constant times Earth's mass) are the model-specific constants, and n_1, n_2 are the minimum and maximum harmonic degree, respectively, of the spectral band being examined. Similarly, the RET potential coefficients $\overline{C}_{nm}^{RET}$ $\overline{S}_{nm}^{RET}$ are evaluated to give gravity disturbances δg^{RET} implied by the uncompensated RET:

$$\delta g^{RET} = \frac{GM}{r^2}\sum_{n=n_1}^{n_2}\left(\frac{a}{r}\right)^n (n+1)\sum_{m=0}^{n}\left(\overline{C}_{nm}^{RET}\cos m\lambda + \overline{S}_{nm}^{RET}\sin m\lambda\right)\cdot\bar{P}_{nm}(\cos\theta) \quad (18)$$

where $GM = GM^{GGM} = 3.986004415 \times 10^{14}$ m^3 s^{-2} for all seven GGMs assessed (Table 1). Accordingly, evaluating equation (18) with the $\overline{C}_{nm}^{A/H}\overline{S}_{nm}^{A/H}$ ($\overline{C}_{nm}^{P/H}\overline{S}_{nm}^{P/H}$) gives gravity disturbances $\delta g^{A/H}$($\delta g^{P/H}$) of the A/H-compensated and P/H-compensated topography, respectively. The gravity $\delta g^{A/H-P/H}$ implied by the combined A/H-P/H model is obtained by using $\delta g^{P/H}$ over the oceans and $\delta g^{A/H}$ elsewhere. Hereafter, we use the general term "gravity" for δg^{GGM}, δg^{RET} and $\delta g^{A/H}$, $\delta g^{P/H}$ and $\delta g^{A/H-P/H}$ from equations (17) and (18).

[36] Equations (17) and (18) were evaluated with the harmonic_synth software (http://earth-info.nga.mil/GandG/wgs84/gravitymod/new_egm/new_egm.html) on the surface of an authalic sphere with radius $r = R = 6378137$ m. This sets the attenuation factor $(a/r)^n$ in equation (18) to unity, while $(a^{GGM}/R)^n$ is very close to unity in equation (17). The $(a^{GGM}/r)^n$ ranges between 0.999973 and 1, because $a^{GGM} - r < 1$ m for all seven GGMs assessed and the smallest possible value of $(a^{GGM}/r)^n$ is 0.999973 (for $n = 250$ and $a^{GGM} = 6378136.3$ m). As a consequence, the attenuation factors only affect our evaluation results by less than 0.003%, which is negligible.

4. Analyses and Results

4.1. Evaluation Criteria

4.1.1. Correlation Coefficients and Reduction Rates

[37] We computed 10′ × 10′ grids of GGM gravity for each GGM in Table 1 over a series of two-degree spectral bands $[n, n+1]$, starting from [2, 3] up to $[n_{\max}-1, n_{\max}]$ the model's maximum degree $n_{\max}$, and then compared these against gravity implied by the (i) uncompensated RET, (ii) A/H-compensated RET, (iii) P/H-compensated RET and (iv) A/H-P/H combined compensated RET in the same bands in the spatial domain.

[38] To evaluate the GGM's spectral content as a function of degree, we use cross-correlation coefficients (CCs) between δg^{GGM} and δg^{RET}, δg^{GGM} and $\delta g^{A/H}$, δg^{GGM} and $\delta g^{P/H}$, and δg^{GGM} and $\delta g^{A/H-P/H}$, respectively. CCs between topography and gravity have been used previously, e.g., by *Rapp* [1982], *Rummel et al.* [1988] and *Wieczorek* [2007], among many others. We also use a new indicator called reduction rates (RRs), given by

$$RR = 100\% \cdot \left(1 - \frac{RMS(\delta g^{REF} - \delta g^{GGM})}{RMS(\delta g^{REF})}\right) \quad (19)$$

where RMS is the root mean square of the δg^{REF} and the differences ($\delta g^{REF} - \delta g^{GGM}$), respectively, and δg^{REF} is the reference signal, which can either be gravity implied by the uncompensated topography (δg^{RET}), by the A/H-compensated topography ($\delta g^{A/H}$), the P/H-compensated topography ($\delta g^{P/H}$), or the combined A/H-P/H-compensated topography $\delta g^{A/H-P/H}$.

[39] Reduction rates (RRs) quantify the extent to which the signal strength of δg^{REF} is reduced ('explained') by the model gravity δg^{GGM} or, in other words, the strength of δg^{REF} signals captured by the δg^{GGM}. Moderate positive RRs (say about 30% to 50%) indicate considerable topography-generated gravity signals are captured by the GGM, whereas RRs near or below 0% show that the GGM signal is unrelated to the topography. Smaller, but positive, RRs (say about 10% to 20%) indicate that the GOCE model contains TIG signals δg^{REF} to some, but limited, extent. RRs close to 80–90% indicate that the GGM signal is almost entirely generated by the modeled topography. However, given the presence of unmodeled mass-density anomalies in the real topography and the Earth's interior, such values do not occur at the spatial scales resolved by GOCE (see sections 4.2 and 4.3). From equation (19), RRs cannot exceed 100%.

[40] Moderate positive RRs always correspond to large positive CCs between δg^{REF} and δg^{GGM}. Conversely, a large positive CC between δg^{REF} and δg^{GGM} does not necessarily correspond to a large RR. In cases where the model is underpowered near the model resolution (due to gravity attenuation at satellite height), we consider it possible that δg^{REF} and δg^{GGM} are strongly correlated (the gravity highs and lows appear at the same locations), but the δg^{GGM} RMS signal strength is smaller than implied by the topography δg^{REF}. Despite larger CCs, RRs will then be low, thus better indicating the deteriorating quality of the model. We have tested RRs extensively using both the δg^{RET}, $\delta g^{A/H}$, $\delta g^{P/H}$ and $\delta g^{A/H-P/H}$ as reference δg^{REF} in equation (19). As a prerequisite for moderate positive RRs, the RMS signal strength of δg^{REF} has to be similar (or larger) than that of the observed gravity δg^{GGM}. Otherwise, the RMS ($\delta g^{REF} - \delta g^{GGM}$) will exceed the RMS($\delta g^{REF}$), failing to indicate topography-generated signals in the GGM.

4.1.2. Effective and Formal Model Resolution

[41] Degree-wise comparisons between quantities derived from spherical harmonic models are always subject to oscillations [e.g., *Rapp*, 1982; *Rummel et al.*, 1988; *Wieczorek*, 2007; *Gruber et al.*, 2011]. Because these oscillations also propagate into quality indicators (be it CCs, RRs or other indicators), and because most of the GGMs contain topographic signals over their entire spectrum, it is generally difficult to discriminate the maximum harmonic

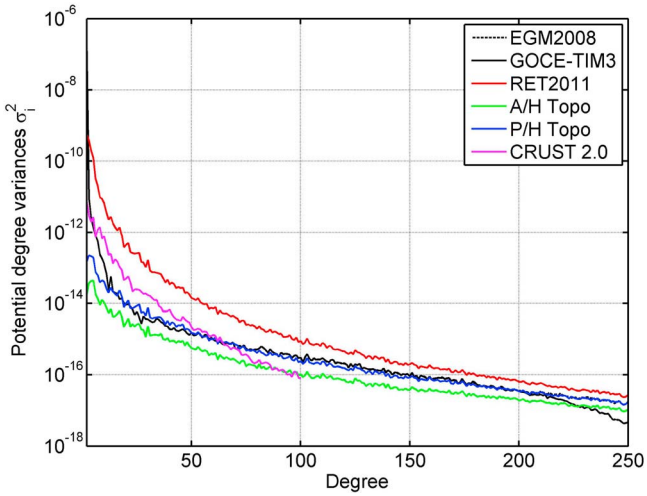

Figure 3. Dimensionless degree variances of selected GGMs and topographic/isostatic models.

degree upon which the GGMs deliver full (i.e., not affected by attenuation) information on Earth's gravity field [see also *Gruber et al.*, 2011; *Hirt et al.*, 2011]. We found that neither the harmonic degree where the RRs are maximum nor constant thresholds (e.g., 20%) are informative numerical criteria because these oscillations vary from region to region. As a compromise, we use the following simple numerical threshold:

$$t = f \times \bar{r} \tag{20}$$

where $f = 0.85$ and $\bar{r}$ is the GGMs average RR in band 100 to 175 over the region under investigation.

[42] What we will term the *effective resolution* is the smallest harmonic degree (but larger than 150) where the GGM's RR falls below our threshold criterion (equation (20)). The effective resolution indicates the degree where the GGMs seem to possess almost full spectral power. Opposed to this, the *formal resolution* is the maximum expansion degree of the GGMs in Table 1. We acknowledge that the criterion in equation (20) is somewhat arbitrary because the choice of factor f influences the threshold and thus the interpreted effective resolution. However, the use of this criterion suppresses the influence of the oscillations (sections 4.2 and 4.3) on the choice of effective resolution because the same criterion applies to all GGMs and they are being compared in a relative manner.

4.2. Preliminary Comparisons

[43] To initially analyze the spectral properties of our data sets, we have computed (dimensionless) potential degree variances σ_n [e.g., *Rapp*, 1982; *Rummel et al.*, 1988]:

$$\sigma_n = \sum_{m=1}^{m} \overline{C}_{nm}^2 + \overline{S}_{nm}^2 \tag{21}$$

where n is the degree, m the order and $\overline{C}_{nm}\,\overline{S}_{nm}$ are the spherical harmonic coefficients of the GGMs, of the uncompensated RET, or of the A/H- or P/H-compensated topography. From Figure 3, the (uncompensated) RET significantly exceeds the spectral power of Earth's observed gravity field, as represented through EGM2008 and GOCE-TIM3. This behavior [e.g., *Rummel et al.*, 1988, Figure 2; *Watts*, 2001, p. 416] shows that the gravitational attraction of isostatic compensation masses and other mass-density anomalies in the Earth's interior "compete" with the attraction of Earth's uncompensated topography, most significantly at long- and medium wavelengths. The A/H compensation model diminishes the spectral power of the uncompensated topography to a level well below that of Earth's observed gravity field [see also *Rummel et al.*, 1988]. Opposed to this, the spectral power of the P/H-compensated topography is very similar to that of Earth's observed gravity field, which is in agreement with *Makhloof* [2007, p. 102].

[44] To gain some insight into the effectiveness of our topography and compensation variants to indicate topography/isostasy-implied signals in the GOCE gravity fields, we compared gravity δg^{GGM} from the highest-resolution space-collected GGM GOCE-TIM3 with δg^{RET}, $\delta g^{A/H}$ and $\delta g^{P/H}$, and with the combined $\delta g^{AH/PH}$ as a function of the spherical harmonic degree over a near-global area ($-83.3° \le \varphi \le 83.3°$ and $-180° \le \lambda \le 180°$). From Figure 4 (top), RRs using the uncompensated RET2011 as a reference are generally larger than RRs using compensated RET. RRs using $\delta g^{P/H}$ as a reference are largest at the long spatial scales, at the 20% level at medium scales and comparable to that of RET2011 beyond degree 200. From Figure 4 (top), P/H appears to better describe isostasy globally at long- and medium scales than A/H. For the combined A/H-P/H model, RRs are larger than of A/H and below those of the P/H.

[45] The CCs for all three topographic/isostatic models agree reasonably well over all harmonic degrees (Figure 4, bottom), and thus do not allow discrimination between the different topographic/isostatic models. Only RRs are capable of discriminating between the topographic/isostatic models (Figure 4, top), and additionally indicate the increasing relevance of topography-generated signals in the observed gravity field (seen by the steadily increasing RRs up to degree ~200). Given that RRs require a reference signal δg^{REF} of sufficient spectral power (see section 4.1.1 and Figure 3), it becomes clear that the underpowered A/H compensated topography does not serve well as reference signal at long and medium spatial scales (seen by the very low or negative RRs for A/H in Figure 4, top). Focusing on spatial scales less than ~100 km (that is, beyond harmonic degree 200), CCs and RRs indicate—irrespective of using uncompensated or compensated topography—a declining amount of topography-generated gravity signals. However, neither the CCs nor RRs indicate that the agreement of GOCE-measured gravity with Earth's topography improves over RET2011 when employing the isostatic compensation models at ~100 km spatial scales.

[46] Neglecting the isostatic compensation masses, the uncompensated RET2011 should theoretically be the poorer representation of Earth's topography/isostasy, while adding isostatic compensation effects to RET2011 should be a theoretically better representation. However, the observation that the isostatic models do not improve the agreement over RET2011-only at medium and short spatial scales suggests that none of the isostatic models included here is a very suitable representation of compensating masses.

[47] For comparison purposes, the Crust.2.0 lithosphere model has been tested as an "observation-based" global

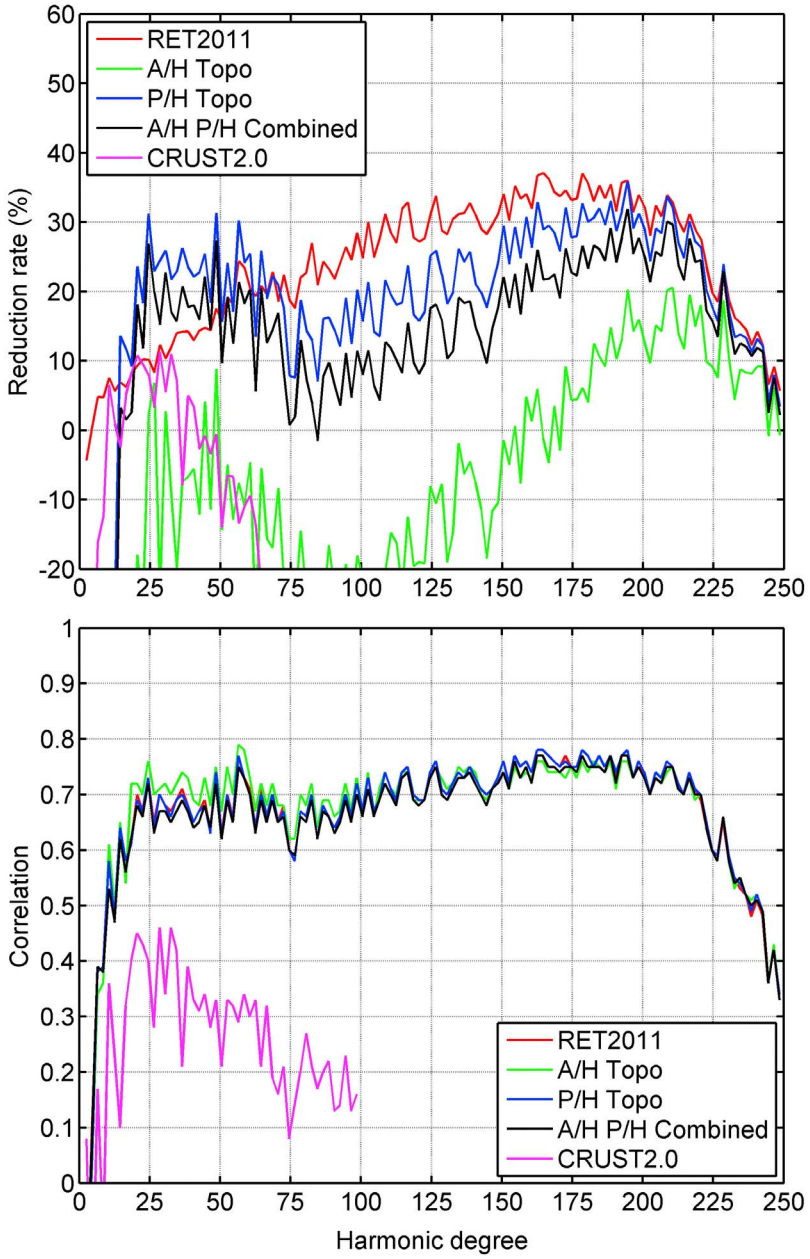

Figure 4. (top) Reduction rates and (bottom) cross-correlation coefficients between GOCE-TIM3 and various topographic/isostatic models as a function of harmonic degree n. Evaluation area is $-83.3° \le \varphi \le 83.3°$ and $-180° \le \lambda \le 180°$.

description of crustal thickness (potential coefficients are from *Kuhn and Featherstone* [2003], derived through spherical harmonic analysis of the upper- middle and lower crustal layers as well as the crust-mantle boundary aka Moho). From Figure 3, Crust 2.0s spectral power ranges between RET and Earth's observed gravity up to harmonic degree ~50, and declines rapidly at medium wavelengths. Comparison among Crust 2.0-implied gravity and the GOCE-observed gravity field (Figure 4) shows generally low CCs (less than +0.5), with the RRs indicating some crustal signals captured by GOCE (through GPS-based orbit determination) between degrees 10 and 40. The Crust.2.0-implied gravity field bears little resemblance to the Earth's gravity field, and fails to deliver meaningful information beyond degree ~40, so is unusable to provide a feedback on the GOCE-measured short-scale gravity field.

[48] We acknowledge that the A/H and P/H isostatic compensation models reduce the differences between Earth's observed gravity field and gravity effects implied by the uncompensated topography regionally to some extent [cf. *Watts*, 2011, Figure 1; *Göttl and Rummel*, 2009, p. 1255]. However, From Figure 4 it is evident that the A/H and P/H models—along with the evaluation methodology applied here—fail to improve the agreement between GOCE and the uncompensated topography globally.

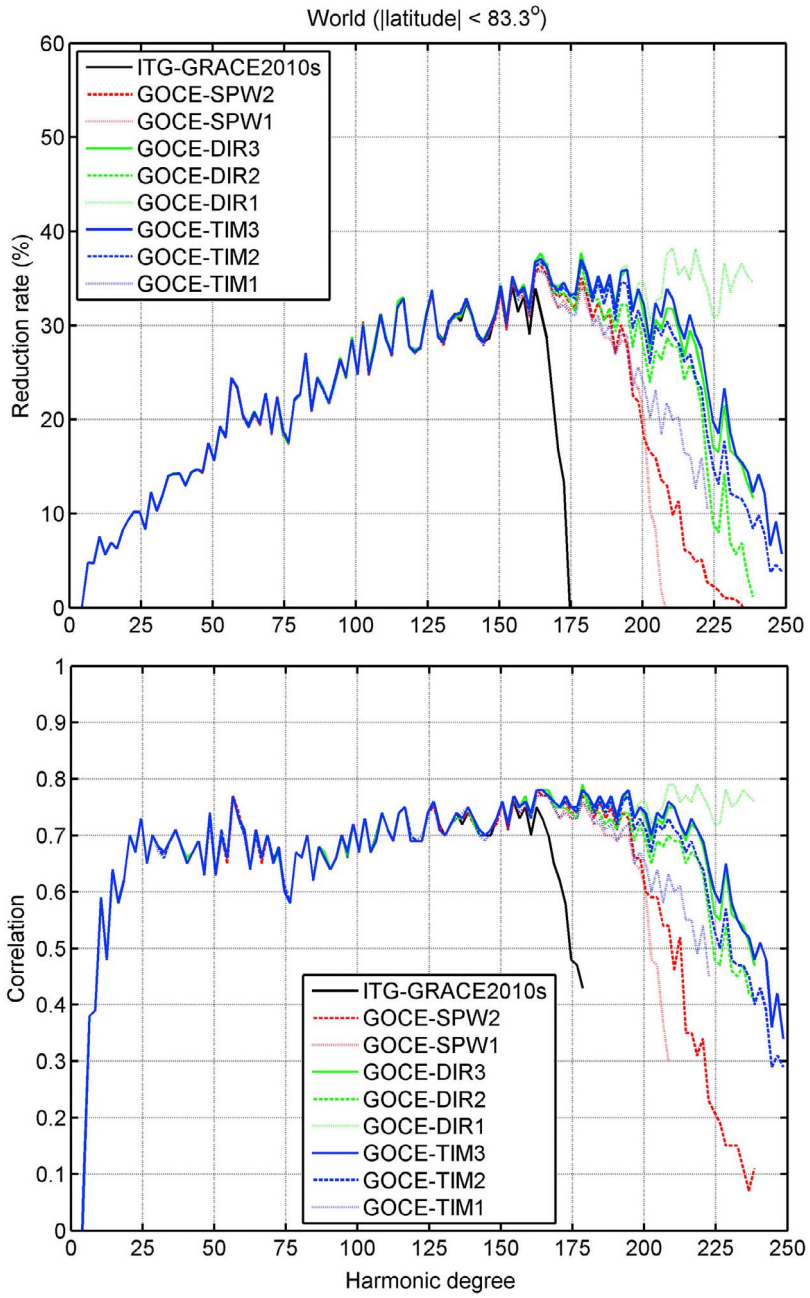

Figure 5. (top) Reduction rates and (bottom) cross-correlation coefficients between RET2011 and GGM gravity as a function of degree n. Evaluation area is $-83.3° \le \varphi \le 83.3°$ and $-180° \le \lambda \le 180°$.

[49] The observation that the A/H and P/H compensation models do not improve the agreement does not necessarily imply that isostatic compensation is not present at all at short, say ~100 km, scales. It only implies that the classical hypotheses are of limited use to accurately model local isostatic compensation globally. We conclude that the A/H and P/H and combined compensation models are not better suited than the uncompensated topography (RET2011) to study the resolution of the new GOCE gravity fields. As a consequence, we use the uncompensated topography δg^{RET} as reference δg^{REF} in our global and regional comparisons in the sequel.

4.3. Near-Global Comparisons With RET2011

[50] The polar regions ($|\varphi| > 83.3°$) that GOCE cannot fly over due to its orbital inclination of 96.7° are excluded from the following comparisons. Figure 5 shows the RRs (top) and CCs (bottom) between $10' \times 10'$ near-global grids of δg^{GGM} and δg^{RET} as a function of degree for each GGM (cf. Table 1). RRs increase to ~35% up to degree ~150, almost identically for all models, showing the increasing strength of topographic gravitational signals captured by the GGMs. Up to degree ~150, neither the CCs nor RRs differ markedly for any of the GGMs. Hence, at low- and medium-

Table 2. Effective Spherical Harmonic Degree for Each GGM (cf. Table 1) as Inferred by Equation (20)

Model	World[a]	Himalayas[b]	Andes[c]	Africa[d]	New Guinea[e]	Antarctica[f]
ITG-Grace2010s	168	172	168	168	166	164
GOCE-SPW2	196	196	180	190	180	196
GOCE-SPW1	196	190	180	176	184	164
GOCE-DIR3	220	200	180	200	196	202
GOCE-DIR2	202	198	180	176	188	190
GOCE-DIR1	n/o[g]	n/o[g]	224	n/o	196	222
GOCE-TIM3	222	208	190	186	200	222
GOCE-TIM2	202	200	190	186	196	202
GOCE-TIM1	196	172	180	176	188	164

[a] $-83.3° \le \varphi \le 83.3°$, $-180° \le \lambda \le 180°$.
[b] $20° \le \varphi \le 45°$, $65° \le \lambda \le 110°$.
[c] $-80° \le \varphi \le -60°$, $-40° \le \lambda \le 10°$.
[d] $-30° \le \varphi \le 30°$, $10° \le \lambda \le 40°$.
[e] $-10° \le \varphi \le 0°$, $130° \le \lambda \le 150°$.
[f] $-83.3° \le \varphi \le -70.0°$, $-180° \le \lambda \le 180°$.
[g] n/o = not observed.

frequencies, both indicators are unable to discriminate among their performance.

[51] Beyond degree ∼150, RRs and CCs start to diverge for all GGMs. This now allows for discrimination among their short-scale agreement with topography-generated gravity signals. The topography is considered to be the dominant source of short-scale gravity field signals [e.g., *Forsberg and Tscherning*, 1981; *Pavlis et al.*, 2007; *Hirt et al.*, 2010b, 2011], which is why an improved agreement between measured and topography-generated gravity can be expected with increasing harmonic degree n. Therefore, the drop in RRs and CCs (Figure 5) indicate that the GGMs lose spectral power, i.e., are increasingly unable to capture the topography-implied gravity signal. From Figure 5, we infer the following:

[52] 1. ITG-GRACE2010s starts losing topography-generated signals near degree ∼160.

[53] 2. All GOCE-GGMs capture topographic signals well up to degree ∼175, with RRs close to ∼40% and CCs near +0.75.

[54] 3. The first-generation GOCE-GGMs SPW1 and TIM1 show a very similar decline in signal between degrees ∼180 and ∼200, while the second- and third-generation GOCE GGMs start losing topography signals between degrees ∼200 and ∼220.

[55] Furthermore:

[56] 1. The performance curves of DIR3 and TIM3, and of DIR2 and TIM2 are very close together, separated from SPW2 by a spectral difference of ∼15 harmonic degrees.

[57] 2. The third-generation DIR3 and TIM3 improve over the second-generation DIR2 and TIM2 in the spectral band of ∼200 to ∼240, where the RRs of the third-generation models are by ∼5% larger than of those of the second generation. TIM3 shows the best agreement with gravity generated by the uncompensated topography.

[58] 3. Even near or at their formal resolution (cf. Table 1), the GOCE GGMs exhibit positive RRs, showing the sensitivity of GOCE for short-scale topography signals, beyond degree ∼200, albeit strongly attenuated. The highest sensitivity for short-scale gravity recovery is visible for DIR3 and TIM3 (positive RRs up to degrees ∼240–250).

[59] 4. DIR1 shows a good agreement with the topography up to its formal resolution of degree 240, but this is because of its high-frequency augmentation with terrestrial data (Table 1).

[60] The effective GGM resolutions, computed from the criterion in equation (20), are reported in Table 2. TIM1 and SPW1 seem to capture most of the topography-generated gravity signals to degree ∼195, which is somewhat larger than assessments based on ground-truth gravity field functionals [cf. *Gruber et al.*, 2011; *Hirt et al.*, 2011]. The second- and third-generation GOCE GGMs possess almost full power to degree ∼200 and ∼220 respectively, which is an improvement over the first-generation GOCE GGMs and over ITG-GRACE2010s from the pre-GOCE-era. From Figure 3, the GOCE TIM3 and EGM2008 degree variances are in close agreement up to degree ∼210–220, which corroborates our results from Figure 5. It should be stressed here that the GGMs spectral content extends beyond their effective resolution; however, gravity field signals are found to be increasingly attenuated. This is within expectation, given that satellite gravimetry cannot sense the high-frequency gravity field because of the decaying gravity signals at satellite altitude [e.g., *Kaula*, 1966].

[61] The relation between GOCE- and topography-implied gravity (Figure 3) poses the question why CCs are not greater than ∼+0.7, and only about ∼35% of GOCE-measured gravity is explained by RET at scales of ∼100 km (regionally, these values can be higher, see section 4.2). *Wieczorek* [2007] analyzed the correlation between gravity (from a GRACE-based GGM) and (rock-equivalent) topography, yielding CCs at a similar level of +0.7, which corroborates our results using RET2011. Importantly, CCs are not higher when applying Crust 2.0, or A/H and P/H compensation models, as was shown in Figure 4. We therefore infer that topography-implied gravity (as well as those implied by the hypothesis-based compensated topography, cf. section 4.1) globally explains GOCE-captured gravity to some, but still limited, extent at spatial scales of ∼100 km, and significant crustal mass-density anomalies exist that superimpose the RET2011-generated signals, and those of the A/H and P/H-compensated topography. Given that the topography/isostasy models used here fail to explain the majority of GOCE-captured gravity signals, there is some potential to derive better-resolution models of the lithosphere from GOCE (see the discussion in section 5).

[62] As a further justification for using RRs for GOCE-GGM assessment over CCs, the comparison between the two indicators in Figure 5 shows that CCs are less sensitive to indicate the extent of captured topography signals (seen by the almost constant correlation of +0.7 between degrees ∼25 to ∼150, while RRs steadily increase) and signal loss (CCs range between +0.1 and +0.5, while RRs are equally near 0%). Hence, only the correlation between model and topography-implied gravity cannot be recommended as a sole indicator for GGM analysis.

4.4. Regional Comparisons With RET2011

[63] Figure 6 shows the differences between TIM2 and EGM2008 gravity in the same spectral band of degrees 2 to 200. The agreement is satisfactory over wide parts of the oceans, Europe, North America and Australia (areas where EGM2008 is mostly based on dense altimetric and terrestrial

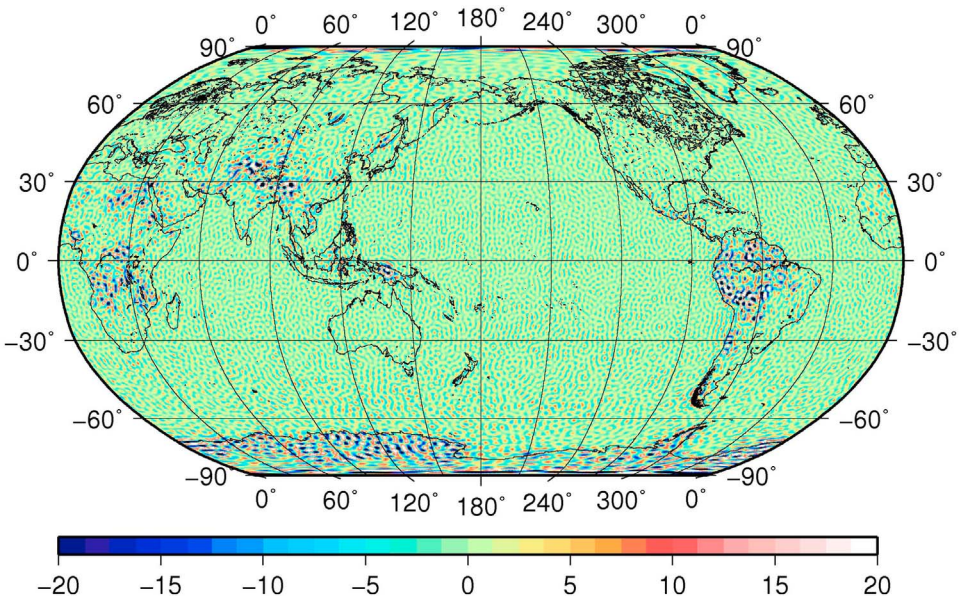

Figure 6. Differences between gravity from EGM2008 and GOCE-TIM2, spectral band 2 to 200, Robinson projection, units in mGal.

gravity data), while large differences are present over parts of Asia, Africa, South America and Antarctica [see also *Hirt et al.*, 2011; *Pail et al.*, 2011; *Rummel et al.*, 2011]. These are regions of rather poor terrestrial gravity availability, and where GOCE is expected to add significantly to gravity field knowledge. It was argued by *Hirt et al.* [2011, p. 735]: "Large differences, occurring over [these] regions … indicate GOCE may improve over EGM2008. However, since there are no ground truth data in these regions, it is only possible to make an inference."

[64] Over the regions in Figure 7, we benchmark GOCE improvements by means of topography-implied gravity with data extending over the entire areas for the first time. Our evaluation offers some compromise in the interim until terrestrial/airborne gravimetry can be collected to provide real ground-truth, or the proprietary data sets [cf. *Pavlis et al.*, 2008] are declassified. We have chosen five regions of relatively poor ground gravity coverage—the Himalayas, Andes, Africa, Papua New Guinea and Antarctica (North of the −83.3° parallel) —which are marked in Figure 2. Over each of these regions, RRs (and for the sake of completeness CCs) are shown in Figure 7. The effective degrees computed from equation (20) are reported in Table 2. In comparison with Figure 5, oscillations of the indicators are stronger, which is due to the limited extent of the test regions. Over all regions, the comparisons between the GOCE GGMs and topography-implied gravity show unanimously that (1) the second (third) generation GOCE gravity values are in close agreement with topography-implied gravity up to degree ∼200 (∼220), (2) the second-generation of GOCE models improves upon the first generation in band ∼185 to ∼200, and (3) GOCE delivers improved gravity field knowledge in band ∼165 to ∼200 compared with GRACE.

[65] Over all regions, the GOCE-TIM2 (TIM3) solution appears to offer the best performance, marginally better than GOCE-DIR2 (DIR3) and notably better than GOCE-SPW2 at short scales. The agreement between topography and DIR1 reflects that it incorporates altimetry and terrestrial gravity data (and, most likely, topography information) in the high spectral degrees. Over the rugged Himalayan and Papua New Guinea areas, RRs are close to ∼50%, indicating that the topography is a dominant source of the gravity field over these areas. Over all of our test regions, GOCE-TIM3 captures RET-implied signals even in harmonic band 240 to 250, which follows from the slightly positive RRs, or, in other words, from the simple observation that subtracting GOCE-TIM3 from RET-implied gravity reduces the RMS-signal strength of the latter (cf. equation (19)). This behavior demonstrates that 12 months satellite gravimetry observations capture information on Earth's gravity field in attenuated form down to ∼80 km spatial scales.

5. Discussion and Conclusions

[66] Degree-wise comparisons between GOCE and gravity implied by Earth's topography show that the second- and third-generation GOCE GGMs add significantly to Earth gravity field knowledge over the Himalayas, Andes, Africa, Papua New Guinea and Antarctica, regions with poor or classified ground gravity coverage and where conventional GGM evaluation can be difficult.

[67] Comparisons were made among eight official ESA GOCE models, based on ∼2, ∼8 and ∼12 months of space-gravimetry observations. These first, second and third-generation GOCE models gradually improve over ITG-GRACE2010s from the pre-GOCE-era, with the third-generation GOCE GGMs enhancing our gravity field knowledge from harmonic degree ∼165 to ∼200–220, or from spatial scales of ∼120 km down to ∼90–100 km, both globally and regionally.

[68] Our comparisons provide some feedback on ESA's three current GOCE gravity recovery philosophies: direct (DIR), time-wise (TIM) and space-wise (SPW), and on the effective model resolution, indicating the highest degree where they seem to possess almost full spectral power.

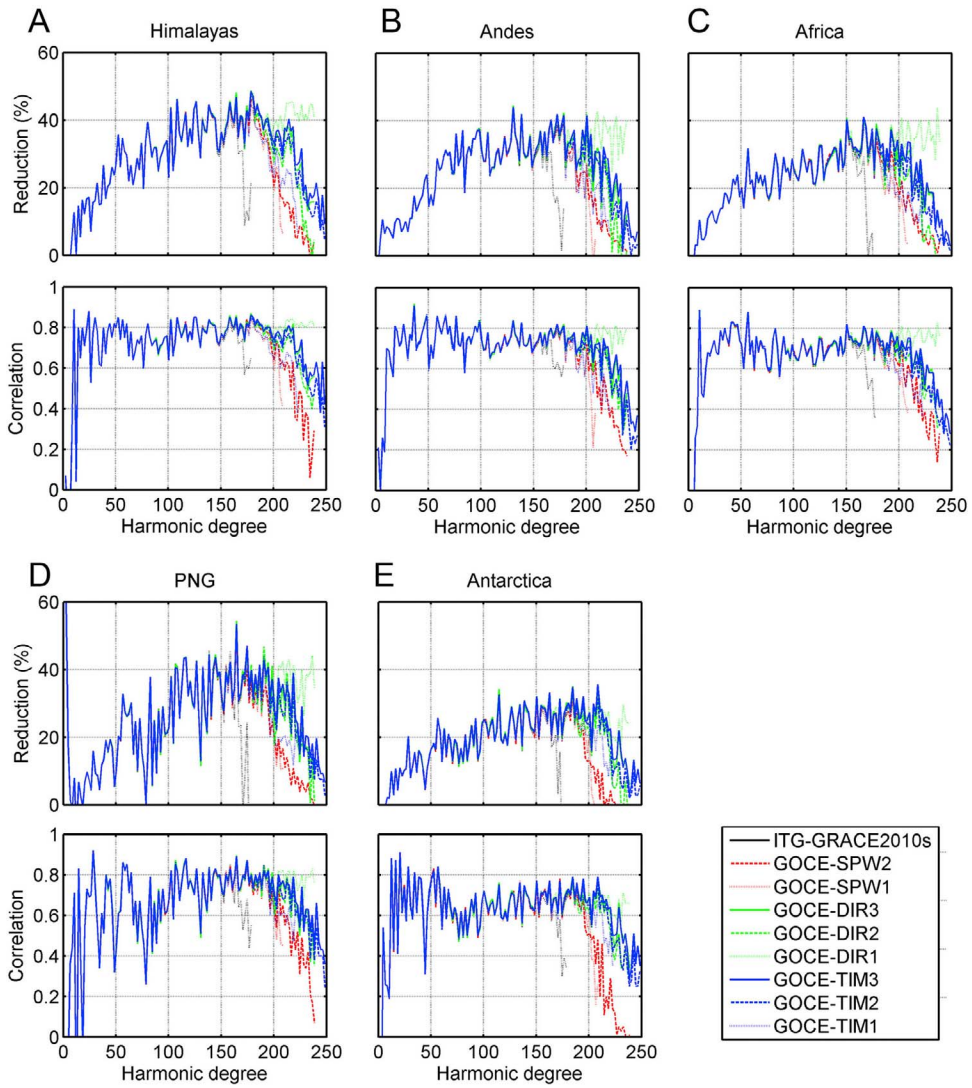

Figure 7. Reduction rates and cross-correlation coefficients between RET2011 and GGM gravity as a function of degree n for five regional study areas: (a) Himalaya ($20° \le \varphi \le 45°$ and $65° \le \lambda \le 110°$), (b) Andes ($-40° \le \varphi \le 10°$ and $-80° \le \lambda \le -60°$), (c) Africa ($-30° \le \varphi \le 30°$ and $10° \le \lambda \le 40°$), (d) Papua New Guinea (PNG) ($-10° \le \varphi \le 0°$ and $130° \le \lambda \le 150°$), (e) Antarctic ($-83.3° \le \varphi \le -70.0°$ and $-180° \le \lambda \le 180°$); the legend for all panels is shown in the bottom right.

Based on second-generation comparisons, the TIM and DIR approaches offer a better agreement with topography-implied signals than the SPW approach. Both for the second- and third-generation models, the TIM and DIR approaches showed similarly close agreement with topography-implied gravity, and the third-generation GOCE models were found to capture most of topography-generated gravity field signal to spherical harmonic degrees of ~200–220.

[69] Despite being theoretically a poorer description of the Earth's uppermost mass distribution, the uncompensated topography turned out to be a data source that seems suitable for providing feedback on GOCE gravity field models. The spatial resolution of current lithosphere models based on observations (from seismic refraction data or elastic thicknesses estimates) is not fine enough to provide a feedback on the GOCE gravity models everywhere on Earth.

[70] Therefore, in the absence of better strategies, isostasy was tested based on the classical though simplistic models of Airy/Heiskanen and Pratt/Hayford, and a hybrid combination of them, because these hypotheses [formally] offer a spatial resolution commensurate with GOCE. However, failing to confer improvements over the agreement seen among GOCE and the uncompensated topography, the isostasy models tested here – specifically the A/H hypothesis – are of limited benefit to precisely describe isostasy globally at the spatial scales resolved by GOCE.

[71] In the absence of an efficient high-resolution description of isostasy, the new GOCE gravity field models may become an important new data source that implicitly contain information on yet unknown mass-density features [cf. *Benedek and Papp*, 2009; *Braitenberg et al.*, 2010]. In modeling the density structure of the lithosphere, the

GOCE models may serve as an important boundary condition [cf. *Marotta*, 2003]. The use of GOCE gravity observations specifically for improved recovery of crustal thicknesses (Moho recovery) has been proposed or is under investigation [e.g., *Braitenberg et al.*, 2010; *Tedla et al.*, 2010; *Bagherbandi*, 2011; *Köther et al.*, 2012; *Reguzzoni and Sampietro*, 2012].

[72] The third-generation GOCE models resolve the Earth's gravity field at spatial scales not recovered before by other space gravimetry missions. Showing the closest agreement with topography-implied signals, the TIM3 and DIR3 models are recommended as "currently the best" medium-wavelength space-collected data sources to describe the gravity field over some regions. Further improvements should be anticipated from future GOCE model generations that are based on data volumes larger than ∼12 months.

[73] At spatial scales as short as ∼80–90 km (harmonic degrees of 220 to 250), our comparisons revealed topography-generated gravity signals captured (albeit in attenuated form) by the third-generation GOCE gravity field models. This demonstration of GOCE's ability for short-scale signal recovery down to ∼80–90 km scales suggests that short-wavelength gravity signals originating from e.g., the crust-mantle boundary and buried anomalous mass loads are captured as well, making the new GOCE data sets a promising source to improve our knowledge on the Earth's lithospheric structure.

[74] **Acknowledgments.** We would like to thank the Australian Research Council (ARC) for funding through discovery project grants DP0663020 and DP120102441. M.K. is the recipient of a Curtin Research Fellowship. We also thank the Editor and reviewers for their comments on the manuscript, directing us to include isostatic compensation models in this study. We thank ESA for making the new GOCE gravity fields freely available. Thanks go also to the EGM2008 development team for the topography data. Some figures were produced using the Generic Mapping Tools (GMT) [*Wessel and Smith*, 1998].

References

Abdalati, W., et al. (2010), The ICESat-2 Laser Altimetry Mission, *Proc. IEEE*, *98*(5), 735–751, doi:10.1109/JPROC.2009.2034765.

Amante, C., and B. W. Eakins (2009), ETOPO1 1 arc-minute global relief model: Procedures, data sources and analysis, *NOAA Tech. Memo.*, *NESDIS NGDC-24*, 19 pp.

Bagherbandi, M. (2011), An isostatic Earth crustal model and its applications, PhD dissertation, Div. of Geod. and Geoinf., R. Inst. of Technol., Stockholm, Sweden. [Available at Kth.diva-portal.org/smash/get/diva2:407999/FULLTEXT01.]

Bamber, J. L., R. L. Layberry, and S. P. Gogenini (2001), A new ice thickness and bed data set for the Greenland ice sheet: 1. Measurements, data reduction, and errors, *J. Geophys. Res.*, *106*(D24), 33,773–33,780, doi:10.1029/2001JD900054.

Bassin, C., G. Laske, and T. G. Masters (2000), The currrent limits of resolution for surface wave tomography in North America, *Eos Trans. AGU*, *81*, F897.

Benedek, J., and G. Papp (2009), Geophysical inversion of on board satellite gradiometer data: A feasibility study in the Alpaca region, central Europe, *Acta Geod. Geophys. Hung*, *44*(2), 179–190, doi:10.1556/AGeod.44.2009.2.4.

Bock, H., A. Jaeggi, U. Meyer, P. Visser, J. van den Ijssel, T. van Helleputte, M. Heinze, and U. Hugentobler (2011), GPS-derived orbits for the GOCE satellite, *J. Geod.*, *85*(11), 807–818, doi:10.1007/s00190-011-0484-9.

Braitenberg, C., P. Mariani, M. Reguzzoni, and N. Ussami (2010), GOCE observations for detecting unknown tectonic features, paper presented at Living Planet Symposium, Eur. Space Agency, Bergen, Norway, 27 June to 2 July.

Bruinsma, S. L., J. C. Marty, G. Balmino, R. Biancale, C. Förste, O. Abrikosov, and H. Neumayer (2010a), GOCE gravity field recovery by means of the direct Numerical method, paper presented at Living Planet Symposium, Eur. Space Agency, Bergen, Norway, 27 June to 2 July.

Bruinsma, S. L., J. M. Lemoine, R. Biancale, and N. Vales (2010b), CNES/GRGS 10-day gravity field models (release 2) and their evaluation, *Adv. Space Res.*, *45*(4), 587–601, doi:10.1016/j.asr.2009.10.012.

Colombo, O. L. (1981), Numerical methods for harmonic analysis on the sphere, *Rep. 310*, Dep. of Geod. Sci., Ohio State Univ., Columbus.

Drinkwater, M. R., R. Floberghagen, R. Haagmans, D. Muzi, and A. Popescu (2003), GOCE: ESA's first Earth Explorer Core mission, in *Earth Gravity Field From Space: From Sensors to Earth Sciences*, *Space Sci. Ser. ISSI*, vol. 17, edited by G. B. Beutler et al., pp. 419–432, Kluwer Acad., Dordrecht, Netherlands.

Farr, T. G., et al. (2007), The Shuttle Radar Topography Mission, *Rev. Geophys.*, *45*, RG2004, doi:10.1029/2005RG000183.

Forsberg, R., and C. C. Tscherning (1981), The use of height data in gravity field approximation by collocation, *J. Geophys. Res.*, *86*(B9), 7843–7854, doi:10.1029/JB086iB09p07843.

Förste, C., et al. (2011), EIGEN-6: A new combined global gravity field model including GOCE data from the collaboration of GFZ-Potsdam and GRGS-Toulouse, *Geophys. Res. Abstr.*, *13*, EGU2011-3242-2.

Goiginger, H., et al. (2011), The combined satellite-only global gravity field model GOCO02S, *Geophys. Res. Abstr.*, *13*, EGU2011-10571.

Göttl, F., and R. Rummel (2009), A geodetic view on isostatic models, *Pure Appl. Geophys.*, *166*(8–9), 1247–1260, doi:10.1007/s00024-004-0489-x.

Gruber, T., P. N. A. M. Visser, C. Ackermann, and M. Hosse (2011), Validation of GOCE gravity field models by means of orbit residuals and geoid comparisons, *J. Geod.*, *85*(11), 845–860, doi:10.1007/s00190-011-0486-7.

Heiskanen, W. A., and H. Moritz (1967), *Physical Geodesy*, W.H. Freeman, San Francisco, Calif.

Hirt, C., W. E. Featherstone, and U. Marti (2010a), Combining EGM2008 and SRTM/DTM2006.0 residual terrain model data to improve quasigeoid computations in mountainous areas devoid of gravity data, *J. Geod.*, *84*(9), 557–567, doi:10.1007/s00190-010-0395-1.

Hirt, C., U. Marti, B. Bürki, and W. E. Featherstone (2010b), Assessment of EGM2008 in Europe using accurate astrogeodetic vertical deflections and omission error estimates from SRTM/DTM2006.0 residual terrain model data, *J. Geophys. Res.*, *115*, B10404, doi:10.1029/2009JB007057.

Hirt, C., T. Gruber, and W. E. Featherstone (2011), Evaluation of the first GOCE static gravity field models using terrestrial gravity, vertical deflections and EGM2008 quasigeoid heights, *J. Geod.*, *85*(10), 723–740, doi:10.1007/s00190-011-0482-y.

Janák, J., F. Wild-Pfeiffer, and B. Heck (2012), Smoothing the gradiometric observations using different topographic–isostatic models: A regional case study, in *VII Hotine-Marussi Symposium on Mathematical Geodesy*, *Int. Assoc. Geod. Symp. Ser.*, vol. 137, edited by N. Sneeuw et al., pp. 245–250, Springer, New York, doi:10.1007/978-3-642-22078-4_37.

Kaula, W. M. (1966), *Theory of Satellite Geodesy*, Blaisdel, Waltham, Mass.

Köther, N., H.-J. Götze, B. D. Gutknecht, T. Jahr, G. Jentzsch, O. H. Lücke, R. Mahatsente, R. Sharm, and S. Zeumann (2012), The seismically active Andean and Central American margins: Can satellite gravity map lithospheric structures?, *J. Geodyn.*, doi:10.1016/j.jog.2011.11.004, in press.

Kuhn, M., and W. E. Featherstone (2003), On the optimal spatial resolution of crustal mass distributions for forward gravity field modelling, in *Proceedings of the 3rd Meeting of the International Gravity and Geoid Commission*, edited by I. Tziavos, pp. 195–200, Ziti Ed., Thessaloniki, Greece.

Lythe, M. B., and D. G. Vaughan and BEDMAP consortium (2000), BEDMAP–bed topography of the Antarctic, *BAS Misc. 9*, scale 1:10,000,000, Br. Antarct. Surv., Cambridge, U. K.

Makhloof, A. A. (2007), The use of topographic-isostatic mass information in geodetic applications, Ing dissertation, Inst. für Geod. und Geoinfor., Univ. Bonn, Bonn, Germany.

Makhloof, A. A., and K.-H. Ilk (2008), Effects of topographic–isostatic masses on gravitational functionals at the Earth's surface and at airborne and satellite altitudes, *J. Geod.*, *82*(2), 93–111, doi:10.1007/s00190-007-0159-8.

Marotta, A. (2003), Benefits from GOCE within solid Earth geophysics, *Space Sci. Rev.*, *108*, 95–104, doi:10.1023/A:1026273832697.

Migliaccio, F., M. Reguzzoni, F. Sanso, C. C. Tscherning, and M. Veicherts (2010), GOCE data analysis: The space-wise approach and the first space-wise gravity field model, paper presented at Living Planet Symposium, Eur. Space Agency, Bergen, Norway, 27 June to 2 July.

Mladek, F. (2006), Hydrostatische Isostasie, *Rep. IAPG/FESG 24*, Inst. für Astron. und Physik. Geod., Munich, Germany. [Available at http://www.iapg.bv.tum.de/mediadb/9853/9854/iapg_fesg_rpt_24.pdf.]

Novák, P., and E. W. Grafarend (2006), The effect of topographical and atmospheric masses on spaceborne gravimetric and gradiometric data, *Stud. Geophys. Geod.*, *50*(4), 549–582, doi:10.1007/s11200-006-0035-7.

Pail, R., et al. (2010), Combined satellite gravity field model GOCO01S derived from GOCE and GRACE, *Geophys. Res. Lett.*, *37*, L20314, doi:10.1029/2010GL044906.

Pail, R., et al. (2011), First GOCE gravity field models derived by three different approaches, *J. Geod.*, *85*(11), 819–843, doi:10.1007/s00190-011-0467-x.

Pavlis, N. K., J. K. Factor, and S. A. Holmes (2007), Terrain-related gravimetric quantities computed for the next EGM, paper presented at 1st International Symposium of the International Gravity Field Service, Istanbul.

Pavlis, N. K., S. A. Holmes, S. C. Kenyon, and J. K. Factor (2008), An Earth gravitational model to degree 2160: EGM2008, paper presented at General Assembly of the European Geoscience Union, Vienna, Austria, 13–18 April.

Rapp, R. H. (1982), Degree variances of the Earth's potential, topography and its isostatic compensation, *Bull. Geod.*, *56*(2), 84–94, doi:10.1007/BF02525594.

Reguzzoni, M., and D. Sampietro (2012), Moho estimation using GOCE Data: A numerical simulation, in *Geodesy for Planet Earth*, *Int. Assoc. Geod. Symp. Ser.*, vol. 136, edited by S. Kenyon, pp. 205–214, Springer, New York, doi:10.1007/978-3-642-20338-1_25.

Rummel, R., R. H. Rapp, H. Sünkel, and C. C. Tscherning (1988), Comparisons of global topographic/isostatic models to the Earth's observed gravity field, *Rep. 388*, Dep. Geod. Sci., Ohio State Univ., Columbus.

Rummel, R., W. Yi, and C. Stummer (2011), GOCE gravitational gradiometry, *J. Geod.*, *85*(11), 777–790, doi:10.1007/s00190-011-0500-0.

Saleh, J., and N. K. Pavlis (2003), The development and evaluation of the global digital terrain model DTM2002, in *Proceedings of the 3rd Meeting of the International Gravity and Geoid Commission*, edited by I. Tziavos, pp. 207–212, Ziti Ed., Thessaloniki, Greece.

Smith, W. H. F., and D. T. Sandwell (1997), Global sea floor topography from satellite altimetry and ship depth soundings, *Science*, *277*, 1956–1962, doi:10.1126/science.277.5334.1956.

Tapley, B. D., S. Bettadpur, M. Watkins, and C. Reigber (2004), The gravity recovery and climate experiment: Mission overview and early results, *Geophys. Res. Lett.*, *31*, L09607, doi:10.1029/2004GL019920.

Tedla, G. E., M. van der Meijde, and A. Nyblade (2010), Crustal modeling in Africa: Towards high resolution models using GOCE satellite gravity data, Abstract #T31C-2188 presented at 2010 Fall Meeting, AGU, San Francisco, Calif., 13–17 Dec.

Torge, W. (2001), *Geodesy*, 3rd ed., de Gruyter, Berlin.

Watts, A. B. (2001), *Isostasy and Flexure of the Lithosphere*, Cambridge Univ. Press, New York.

Watts, A. B. (2011), Isostasy, in *Encyclopedia of Solid Earth Geophysics*, edited by H. K. Gupta, pp. 647–662, Elsevier, New York.

Wessel, P., and W. H. F. Smith (1998), New, improved version of the Generic Mapping Tools released, *Eos Trans. AGU*, *79*, 579, doi:10.1029/98EO00426.

Wieczorek, M. A. (2007), The gravity and topography of the terrestrial planets, in *Treatise on Geophysics*, vol. 10, edited by T. Spohn and G. Schubert, pp. 165–206, Elsevier-Pergamon, Oxford, U. K.

Wild, F., and B. Heck (2005), A comparison of different isostatic models applied to satellite gravity gradiometry, in *Gravity, Geoid and Space Missions*, *Int. Assoc. Geod. Symp. Ser.*, vol. 129, edited by C. Jekeli et al., pp. 230–235, Springer, New York.